Supplement of Atmos. Chem. Phys. Discuss., 15, 19947–20011, 2015
http://www.atmos-chem-phys-discuss.net/15/19947/2015/
doi:10.5194/acpd-15-19947-2015-supplement

Atmospheric Chemistry and Physics Discussions

Supplement of

Development of an atmospheric N_2O isotopocule model and optimization procedure, and application to source estimation

K. Ishijima et al.

Correspondence to: K. Ishijima (ishijima@jamstec.go.jp)

1 Model data sampling

To extract model results of atmospheric N_2O mole fraction and isotopocule ratios at the same day and location as those of the observations, daily mean model output data were interpolated using the distances from four model grids surrounding the location of the observation. We did not use the latitude and longitude, because the shape of a model grid changes from quadrangle to trapezoid or triangle poleward. Vertically, we linearly interpolated the model results using simulated geopotential altitudes. Therefore, a sampled model result is basically the interpolation of the model results from eight grids surrounding the observation point.

2 Processing of observed time-series

2.1 Processing of ground-based observation data

A digital low-pass filtering technique by Nakazawa et al. (1997) was used to process observation data from NMY, and AGAGE stations (CGO, MHD, CMO, THD, RPB, and SMO), and then the derived long-term variations were temporally averaged for the period 1991-1998, which are used in Fig. 7. As the input data for the digital filtering, the raw data from NMY and monthly mean (including pollution) data from AGAGE stations were used. As the input time information, the dates of each observation and of the middle of the month were used for NMY and AGAGE stations, respectively.

In the digital filtering process, the observed time-series was represented by a fitted curve, which consisted of the approximate long-term trend represented by a Reinsch-type cubic spline function with a cutoff period of 5 years (LS), the average seasonal cycle by a Fourier function (SF), and short- and long-term components obtained through the Butterworth filters with respective cut off periods of 4 and 36 months (SB and LB). Thus we regarded the long-term variation of the observation data as sum of the approximate long-term trend and the long-term component (LS+LB).

2.2 Processing of firn air analysis data

Histories of atmospheric N_2O mole fraction, $\delta^{15}N^{bulk}$ and $\delta^{18}O$ were reconstructed for the period 1952-2001, based on the analyses of firn air collected at NGRIP (NGR), Greenland, and Dome

Fuji (DFJ) and H72, Antarctica (Ishijima et al, 2007). Since number of the reconstructed firn data for the period of the observation at NMY (1990-2002) was not so many (19, 8, and 10 for NGR, DFJ and H72, respectively), we needed a special data handling to make effective use of the firn data. First, the data from DFJ and H72 were grouped into a dataset for the Northern Hemisphere since the two firn air sampling sites were both in Antarctica, and thereby number of data for the both hemispheres became comparable. Then, the time-series data were fitted by a cubic spline function with a cutoff period of 15 years, and the fitted curves are averaged for the period 1991-1998. These operations slightly improved the reliability for the finally obtained interpolar differences of atmospheric N_2O mole fraction, $\delta^{15}N^{bulk}$ and $\delta^{18}O$ (for 1991-1998). Thus obtained mean values were used in model optimization for atmospheric north-to-south gradient and the Northern Hemisphere to Southern Hemisphere emission ratio described below.

3 Model optimization for tropospheric values

Model optimization for tropospheric N_2O isotopocules consisted of the first step of optimizing the tropospheric long-term trends (and the global total emissions; Sect. 3.1), and the second step of optimizing the tropospheric north-to-south gradients (and the Northern Hemisphere to Southern Hemisphere emission ratios; Sect. 3.2). The two step optimization calculation for the troposphere (Fig. 2 in the main text) was actually done in one program. In this chapter, we explain the each step.

3.1 Model optimization for tropospheric long-term trend and global total emissions

1. Mole fraction, $\delta^{18}O$, $\delta^{15}N^{\alpha}$ and $\delta^{15}N^{\beta}$ of tropospheric N_2O observed on 13 days at NMY station were converted to the mole fractions of $^{14}N^{14}N^{16}O$, $^{14}N^{15}N^{16}O$, $^{15}N^{14}N^{16}O$, and $^{14}N^{14}N^{18}O$ (Sects. 2.1 and 2.2 in the main text).
2. Model results of $^{14}N^{14}N^{16}O$, $^{14}N^{15}N^{16}O$, $^{15}N^{14}N^{16}O$ and $^{14}N^{14}N^{18}O$ at NMY for the observation days were sampled from daily mean model outputs of 16 different scenario simulations (Fig. 2 in the main text) ([small or large initial mole fraction] * [small or large global emission] * [small or large Northern Hemisphere to Southern Hemisphere emission ratio (E_{NH}:E_{SH})] * [small or large photolytic fractionation]; 2 * 2 * 2 * 2 = 16).

3. The model was optimized by combining the small and large initial mole fraction and global emission simulation results to reproduce the observational data at NMY, separately for each N_2O isotopocule and for each of four simulation cases (small and large E_{NH}:E_{SH} ratios and photolytic fractionations). Here, we define that "C" is the simulated mole fraction on an observation day for an isotopocule, and the first and second subscripts of the C indicate that from small (S) or large (L) global emission and initial mole fraction case simulations, respectively (e.g. $C_{L,\,S}$ is a result of an isotopocule mole fraction simulated using large global emission and small initial mole fraction). The model result, finally obtained by the optimization, is presented as follows,

$$C_S = f_E\, C_{S,\,S} + (1 - f_E)\, C_{L,\,S} \quad (1)$$

$$C_L = f_E\, C_{S,\,L} + (1 - f_E)\, C_{L,\,L} \quad (2)$$

$$C_{opt} = f_I\, C_S + (1 - f_I)\, C_L \quad (3)$$

Here, C_S and C_L are the mole fraction results simulated with small and large initial mole fractions, respectively, f_E and f_I are scaling factors, and C_{opt} is the finally optimized model mole fraction. A combination of optimal values of f_E and f_I was determined for each isotopocule so that $\sum_i^{13}\left(C_{model_i} - C_{observation_i}\right)^2$ (C_{XXXi}: mole fraction for observation or model at each data point i) was minimized. Considering the possibility that the f values become out of 0 to 1, the initial ranges for searching the optimal f values were set to a relatively wide range of –1 to 2. The optimal f values were searched by sequentially changing the values, the intervals and ranges being gradually reduced. In the actual calculation, the first guess of the combination ($f_{E,\,1}$ and $f_{I,\,1}$) was obtained with an accuracy of 0.3 in the range of –1 to 2, the second guess ($f_{E,\,2}$ and $f_{I,\,2}$) with an accuracy of 0.15 in the ranges of $f_{E,\,1}$±0.75 and $f_{I,\,1}$±0.75, the third guess ($f_{E,\,3}$ and $f_{I,\,3}$) with an accuracy of 0.075 in the ranges of $f_{E,\,2}$±0.375 and $f_{I,\,2}$±0.375, and the final results were obtained with an accuracy better than 10^{-10}. All results for the f values eventually became between 0 and 1. Finally obtained global emission is as follows,

$$E_{opt} = f_E\, E_S + (1 - f_E)\, E_L \quad (4)$$

Here, E_{opt}, E_S and E_L are the global emission optimized, and of small and large cases for each isotopic component, respectively.

The uncertainties in the mole fraction (C) and global emission (E), caused by this optimization method, were estimated using a Monte Carlo approach for the f values, by assigning random

errors to the observational data and optimizing with the data 100,000 times. The random errors were taken from a Gaussian distribution representing the measurement standard error. The 95% confidence range for the Monte Carlo approach (1.96 * [standard deviation for calculated C_{opt} or E_{opt}]) was regarded as the final uncertainty.

As seen in Fig. 2 in the main text, this optimization was done separately for four cases ([small or large Northern Hemisphere to Southern Hemisphere emission ratio (E_{NH}:E_{SH})] * [small or large photolytic fractionation]; 2 * 2 = 4).

3.2 Model optimization for tropospheric north-to-south gradient and the Northern Hemisphere to Southern Hemisphere emission ratio

In the first step (Sect. 3.1), the model was optimized for the tropospheric long-term trend (and global emission) to reproduce the NMY observational data, separately for four cases (two different E_{NH}:E_{SH} ratios and photolytic fractionations). In the second step, by combining model results of small and large E_{NH}:E_{SH} ratios (already optimized for the long-term trend), tropospheric north-to-south gradient (and E_{NH}:E_{SH} ratio) was optimized, separately for small and large photolytic fractionation cases. For this optimization, mean interpolar differences of tropospheric N_2O mole fraction, $\delta^{15}N^{bulk}$ and $\delta^{18}O$ derived from firn air analyses for the period 1991-1998 (Ishijima et al., 2007; Sect. 2.2 in the Supplement) were used, but that of the $\delta^{15}N^{sp}$ was assumed to be zero, since no data available in this data set (Sect. 4.2.2 in the main text).

1. Before the first optimization (Sect. 3.1), daily mean model mole fractions of $^{14}N^{14}N^{16}O$, $^{14}N^{15}N^{16}O$, $^{15}N^{14}N^{16}O$, and $^{14}N^{14}N^{18}O$ at the three firn stations for all days from Jan 1 1991 to Dec 31 1998 were sampled from 16 scenario simulations (Sect. 3.1; Fig. 2 in the main text). Using the sampled model data and Eqs. (1), (2) and (3) (Sect. 3.1) together with f_E and f_I obtained in the first optimization, mole fractions for the three firn stations, optimized for the long-term trends, were calculated, separately for four cases (small and large E_{NH}:E_{SH} ratios and photolytic fractionations; Fig. 2 in the main text). Then, their temporal means were calculated by simply averaging for the whole period (1991-1998). Here, we regard the mean for NGR (75°N) and mean of the means for DFJ (77°S) and H72 (69°S) as the northern and southern hemispheric values, respectively.

2. We define that "C" is the mean mole fraction of each isotopocule for each hemisphere for 1991-1998, and the first and second subscripts of C indicate that from small (S) or large (L)

E_{NH}:E_{SH} ratio case simulation and for the Northern or Southern Hemisphere, respectively (e.g. $C_{S,\,NH}$ is the mean mole fraction for the Northern Hemisphere for 1991-1998 from the small E_{NH}:E_{SH} ratio simulation). The model result for the Northern Hemisphere (NH) or Southern Hemisphere (NH), which are finally obtained by this optimization, is presented as follows,

$$C_{XH} = f_e \; C_{S,\,XH} + (1 - f_e)\, C_{L,\,XH} \qquad (5)$$

Here, f_e is a scaling factor, and XH means NH or SH.

3. After converting C_{NH} and C_{SH} of four isotopocules to the mole fractions, $\delta^{15}N^{bulk}$, $\delta^{18}O$, and $\delta^{15}N^{sp}$ (Sects. 2.1 and 2.2 in the main text), their interpolar differences (NH-SH) were taken. Here, we define that D_i is the both hemispheric difference of the mole fraction (i=1), $\delta^{15}N^{bulk}$ (i=2), $\delta^{18}O$ (i=3), or $\delta^{15}N^{sp}$ (i=4). Finally, a combination of optimal four f_e values was determined so that $\sum_i^4 \left(D_i^M - D_i^O\right)^2$ was minimized in the same manner as that for f_E and f_I (Sect. 3.1). Here, D^M and D^O are D for model and observation, respectively. Finally obtained E_{NH}:E_{SH} (e) is as follows,

$$e_{opt} = f_e \; e_S + (1 - f_e)\, e_L \qquad (6)$$

Here, e_{opt}, e_S and e_L are the E_{NH}:E_{SH} ratio optimized and of small and large cases for each N_2O isotopocule, respectively.

The uncertainties in the interhemispheric difference (D) and E_{NH}:E_{SH} ratio (e) were estimated in the same manner as that for f_E and f_I (Sect. 3.1), but using uncertainty for the temporal mean of the firn air analysis data (Table 3 in the main text).

As seen in Fig. 2 in the main text, this optimization was done separately for small and large photolytic fractionation cases.

3.3 Tuning of photolytic fractionation

Model optimizations for the troposphere (Sects. 3.1 and 3.2) were done separately for small and large photolytic fractionation cases. Before the tropospheric optimizations (Sects. 3.1 and 3.2), daily mean model mole fractions ($^{14}N^{14}N^{16}O$, $^{14}N^{15}N^{16}O$, $^{15}N^{14}N^{16}O$, and $^{14}N^{14}N^{18}O$) for the day and location of each air sampling in balloon and aircraft observations (Toyoda et al., 2004; Kaiser et al., 2006) were sampled from 16 scenario simulations (Sect. 3.1; Fig. 2 in the main

150 text). Using the sampled model data and Eqs. (1), (2), (3) and (5) together with f_E, f_I, f_1, f_2, f_3,
151 and f_4 (obtained by the tropospheric optimizations; Sects. 3.1 and 3.2), stratospheric mole
152 fraction, $\delta^{18}O$, $\delta^{15}N^{\alpha}$ and $\delta^{15}N^{\beta}$, optimized for the troposphere, were calculated for small and
153 large photolytic fractionation cases. Subsequent procedure is already explained in detail in Sect.
154 4.2.3 in the main text, so only shortly described hereafter. Then, the apparent fractionation
155 constants (Ɛs) were calculated for both small and large photolytic fractionation cases for each
156 of $\delta^{18}O$, $\delta^{15}N^{\alpha}$ and $\delta^{15}N^{\beta}$. Finally, the observed Ɛ ($Ɛ_{obs}$) was linearly-interpolated by using the
157 two Ɛ values from the small ($Ɛ_{org}$) and large ($Ɛ_{red}$) photolytic fractionation simulations (Sect.
158 4.2.3 and Fig. 2 in the main text) and a scaling factor $f_Ɛ$ as follows,

159 $$Ɛ_{obs} = Ɛ_{tun} = f_Ɛ\, Ɛ_{org} + (1 - f_Ɛ)\, Ɛ_{red}, \qquad (7).$$

160 Using the $f_Ɛ$ values, photolysis for $^{14}N^{15}N^{16}O$, $^{15}N^{14}N^{16}O$, and $^{14}N^{14}N^{18}O$ in model were
161 corrected as follows,

162 $$J_{tun} = f_Ɛ\, J_{org} + (1 - f_Ɛ)\, J_{red} = (0.015 f_Ɛ + 0.985)\, J_{org}, \qquad (8)$$

163 Here, J_{tun}, J_{org}, and J_{red} (= 0.985 J_{org}) are photolysis in model for finally corrected (tuned), small
164 (original) and large (1.5 % reduced photolysis) photolytic fractionation cases, respectively.
165

Table S1. Value of f_ε obtained by tuning photolytic fractionation, and the ratio of the tuned photolysis rate to the original photolysis rate for each N_2O isotopocule.

	$^{14}N^{14}N^{16}O$	$^{14}N^{15}N^{16}O$	$^{15}N^{14}N^{16}O$	$^{14}N^{14}N^{18}O$
f_ε	1.00	0.17	0.66	0.69
J_{tun}/J_{org}	1.00	0.9875	0.9950	0.9953

Table S2. Same as Table 4 but for only top-down estimates for 1991-2001 by the ACTM with tuned, original and 1.5% reduced photolysis for $^{14}N^{15}N^{16}O$, $^{15}N^{14}N^{16}O$ and $^{14}N^{14}N^{18}O$.

Area	N_2O (Tg a^{-1} N)	$\delta^{15}N^{bulk}$ (‰)	$\delta^{18}O$ (‰)	$\delta^{15}N^{sp}$ (‰)	Photolysis for $^{14}N^{15}N^{16}O$, $^{15}N^{14}N^{16}O$ and $^{14}N^{14}N^{18}O$
GL	15.5	-10.4	31.2	12.3	Tuned
		-8.6	32.2	13.8	Original
		-11.7	29.0	13.9	1.5% reduced
NH	8.9	-14.6	31.2	(15.1)	Tuned
		-13.5	31.8	(16.0)	Original
		-15.4	29.9	(16.1)	1.5% reduced
SH	6.6	-4.7	31.1	(8.6)	Tuned
		-2.0	32.6	(10.9)	Original
		-6.6	27.8	(11.0)	1.5% reduced

174 Table S3. Mean property of each N_2O isotope for 1991-2001 in optimized model.

	$^{14}N^{14}N^{16}O$	$^{14}N^{15}N^{16}O$	$^{15}N^{14}N^{16}O$	$^{14}N^{14}N^{18}O$	N_2O-sum	*unit*
Total mass	2334.24	8.9221	8.7607	5.1145	2357.03	*Tg N_2O*
Tropospheric mass	2002.32	7.6487	7.5130	4.3856	2021.87	*Tg N_2O*
Stratospheric mass	331.91	1.2734	1.2478	0.7289	335.16	*Tg N_2O*
Total burden	5.4780	2.082E-02	1.999E-02	1.190E-02	5.5307	*Tg a^{-1} N_2O*
Tropospheric burden	4.6611	1.772E-02	1.701E-02	1.013E-02	4.7059	*Tg a^{-1} N_2O*
Stratospheric burden	0.8169	3.104E-03	2.979E-03	1.772E-03	0.8247	*Tg a^{-1} N_2O*
Emission	24.0520	9.005E-02	8.894E-02	5.199E-02	24.2830	*Tg a^{-1} N_2O*
Total loss	18.5740	6.923E-02	6.895E-02	4.009E-02	18.7523	*Tg a^{-1} N_2O*
Tropospheric loss	0.3293	1.217E-03	1.218E-03	7.067E-04	0.3324	*Tg a^{-1} N_2O*
Stratospheric loss	18.2447	6.802E-02	6.773E-02	3.938E-02	18.4198	*Tg a^{-1} N_2O*
Tropospheric photolysis	0.0943	3.290E-04	3.404E-04	1.959E-04	0.0952	*Tg a^{-1} N_2O*
Stratospheric photolysis	16.0696	5.944E-02	5.946E-02	3.454E-02	16.2230	*Tg a^{-1} N_2O*
Tropospheric oxidation	0.2350	8.877E-04	8.775E-04	5.108E-04	0.2372	*Tg a^{-1} N_2O*
Stratospheric oxidation	2.1751	8.574E-03	8.270E-03	4.847E-03	2.1968	*Tg a^{-1} N_2O*
Lifetime	125.67	128.87	127.05	127.58	125.69	*year*
Global mean concentration	300.20	1.1220	1.1017	0.6292	303.06	*nmol mol^{-1}*
Tropospheric mean conc.	309.65	1.1566	1.1360	0.6487	312.60	*nmol mol^{-1}*
Stratospheric mean conc.	253.52	0.9510	0.9319	0.5325	255.94	*nmol mol^{-1}*

	N_2O-sum (*nmol mol^{-1}*)	**$\delta^{15}N^{bulk}$** (*‰*)	**$\delta^{18}O$** (*‰*)	**SP** (*‰*)
Global mean	303.06	7.362	45.191	18.380
Tropospheric mean	312.60	6.911	44.806	18.024
Stratospheric mean	255.94	10.087	47.512	20.526

175

176

177 Table S4. Isotopocule delta values of each source category used in our bottom-up estimation.

178 Means and standard deviations are derived from results compiled by Toyoda et al. (2015).

Source category	Data source	Category in Toyoda et al (2015)	$\delta^{15}N^{bulk}$ (‰)	$\delta^{18}O$ (‰)	$\delta^{15}N^{sp}$ (‰)
Energy manufacturing transformation	EDGRA4.2	Fossil fuel and industry	-10.8 ± 18.3	41.6 ± 11.2	15.8 ± 4.0
Non-road transportation	EDGRA4.2	Fossil fuel and industry	-10.8 ± 18.3	41.6 ± 11.2	15.8 ± 4.0
Road transportation	EDGRA4.2	Fossil fuel and industry	-10.8 ± 18.3	41.6 ± 11.2	15.8 ± 4.0
Residential	EDGRA4.2	Fossil fuel and industry	-10.8 ± 18.3	41.6 ± 11.2	15.8 ± 4.0
Oil production and refineries	EDGRA4.2	Fossil fuel and industry	-10.8 ± 18.3	41.6 ± 11.2	15.8 ± 4.0
Industrial process and product use	EDGRA4.2	Fossil fuel and industry	-10.8 ± 18.3	41.6 ± 11.2	15.8 ± 4.0
Manure management	EDGRA4.2	Manure production	-7.6 ± 4.4	29.6 ± 4.1	11.4 ± 6.5
Agricultural soils	EDGRA4.2	Agricultural soils	-20.8 ± 19.9	26.6 ± 16.8	10.5 ± 9.8
Indirect N2O emissions from agriculture	EDGRA4.2	Agricultural soils	-20.8 ± 19.9	26.6 ± 16.8	10.5 ± 9.8
Agricultural waste burning	EDGRA4.2	Agricultural soils	-20.8 ± 19.9	26.6 ± 16.8	10.5 ± 9.8
Waste solid and wastewater	EDGRA4.2	Human excreta	-14.0 ± 17.1	35.1 ± 14.4	12.4 ± 5.6
Fossil Fuel Fires	EDGRA4.2	Fossil fuel and industry	-10.8 ± 18.3	41.6 ± 11.2	15.8 ± 4.0
Indirect emissions from NOx and NH3	EDGRA4.2	Fossil fuel and industry	-10.8 ± 18.3	41.6 ± 11.2	15.8 ± 4.0
Natural soil	EDGAR2	Natural soils	-14.6 ± 13.9	31.5 ± 18.7	13.2 ± 11.4
Ocean	Nevison et al. (1995) & Jin&Gruber (2003)	Ocean	6.4 ± 4.4	49.0 ± 11.3	13.9 ± 8.3
Biomass burning	GFED3.1	Biomass burning	-3.5 ± 4.4	23.9 ± 1.9	1.6 ± 4.6

179

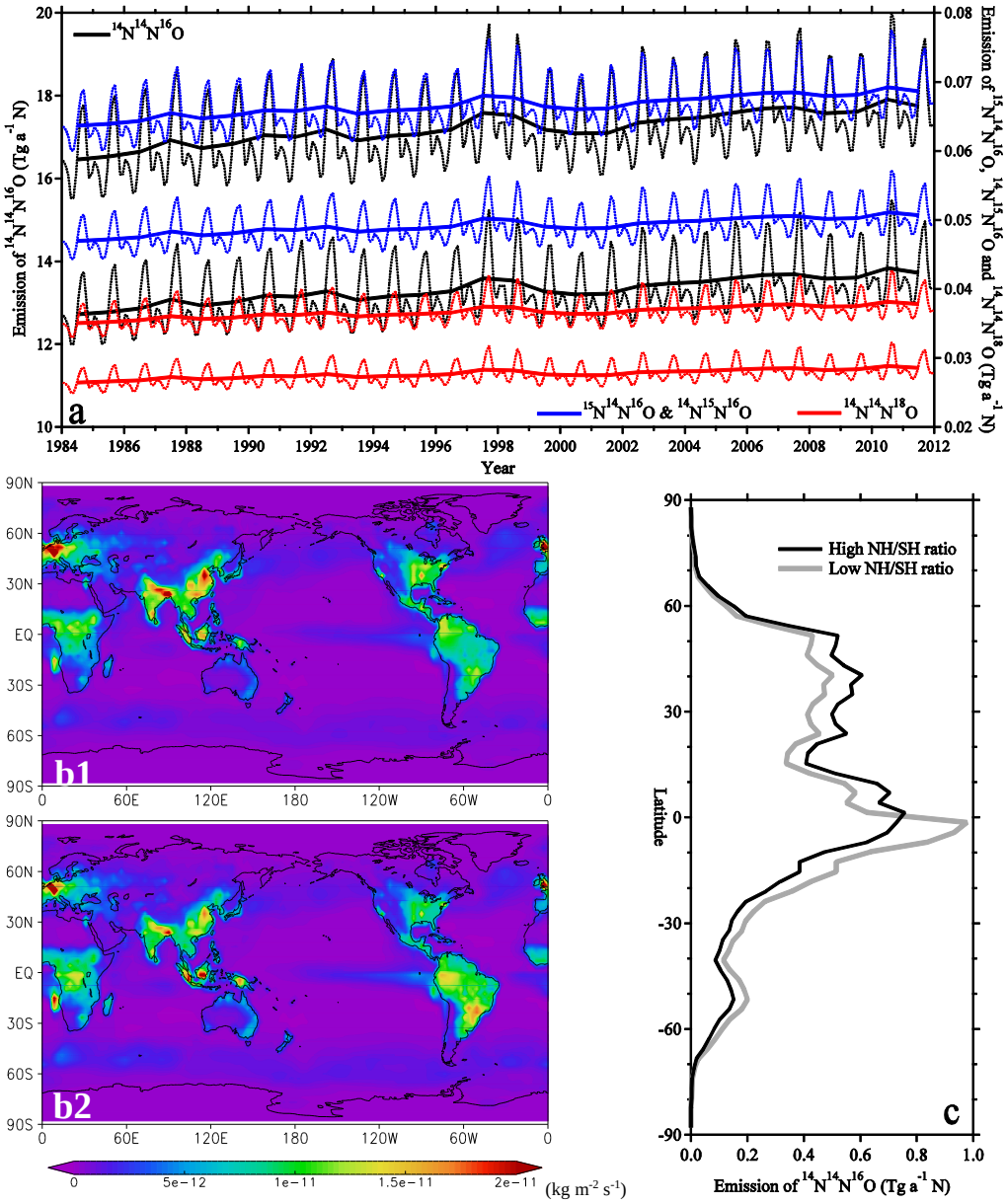

Figure S1. Emissions of N_2O isotopocules used in simulations in this study. (a) Annual (solid line) and monthly (dashed line) mean emissions for small and large emission cases for each N_2O isotopocule (emissions of $^{15}N^{14}N^{16}O$ and $^{14}N^{15}N^{16}O$ are completely same). (b) Mean emission distribution of $^{14}N^{14}N^{16}O$ for large (1) and small (2) Northern Hemisphere to Southern Hemisphere emission ratio cases for the period 1991-2001, and their latitudinal distributions (c). Temporal and horizontal emission patterns are same for all isotopes, but scaled by different factors.

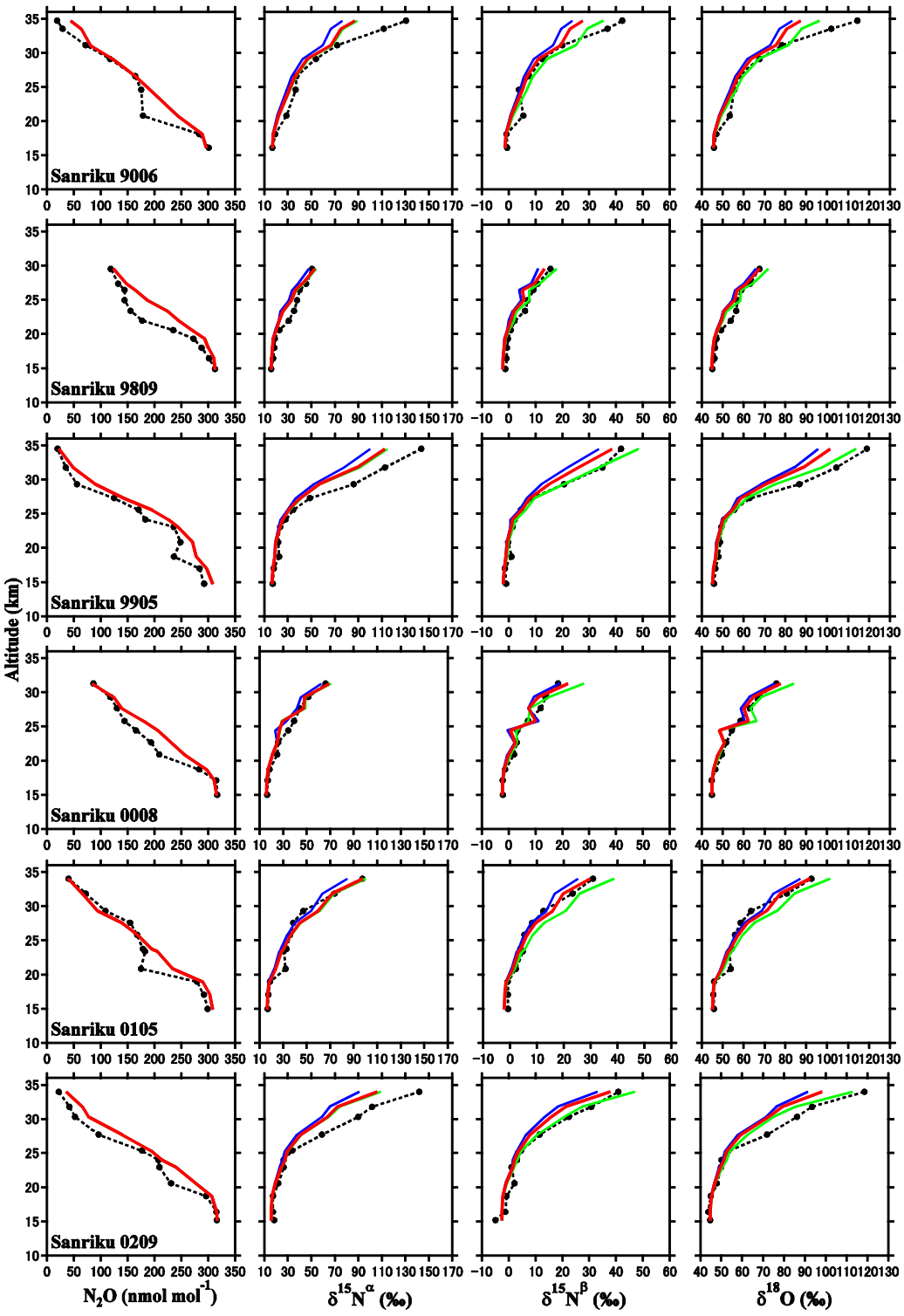

Figure S2 (a). Same as Fig. 6, but for N_2O mole fraction, $\delta^{15}N^{\alpha}$, $\delta^{15}N^{\beta}$ and $\delta^{18}O$ from all balloon and aircraft observations, which were used for the optimization of photolytic fractionation in the model.

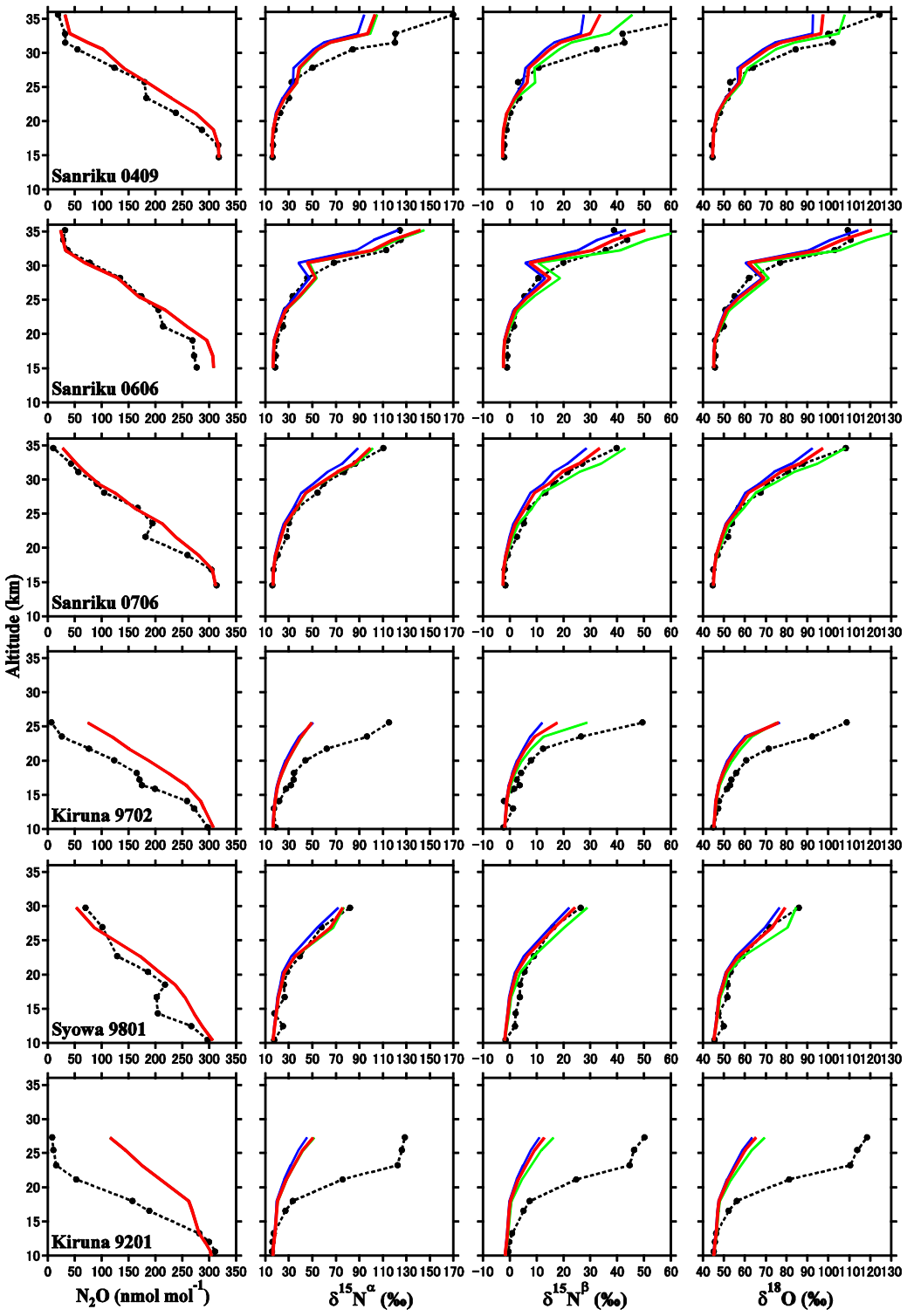

195

196

197 Figure S2 (b).

198

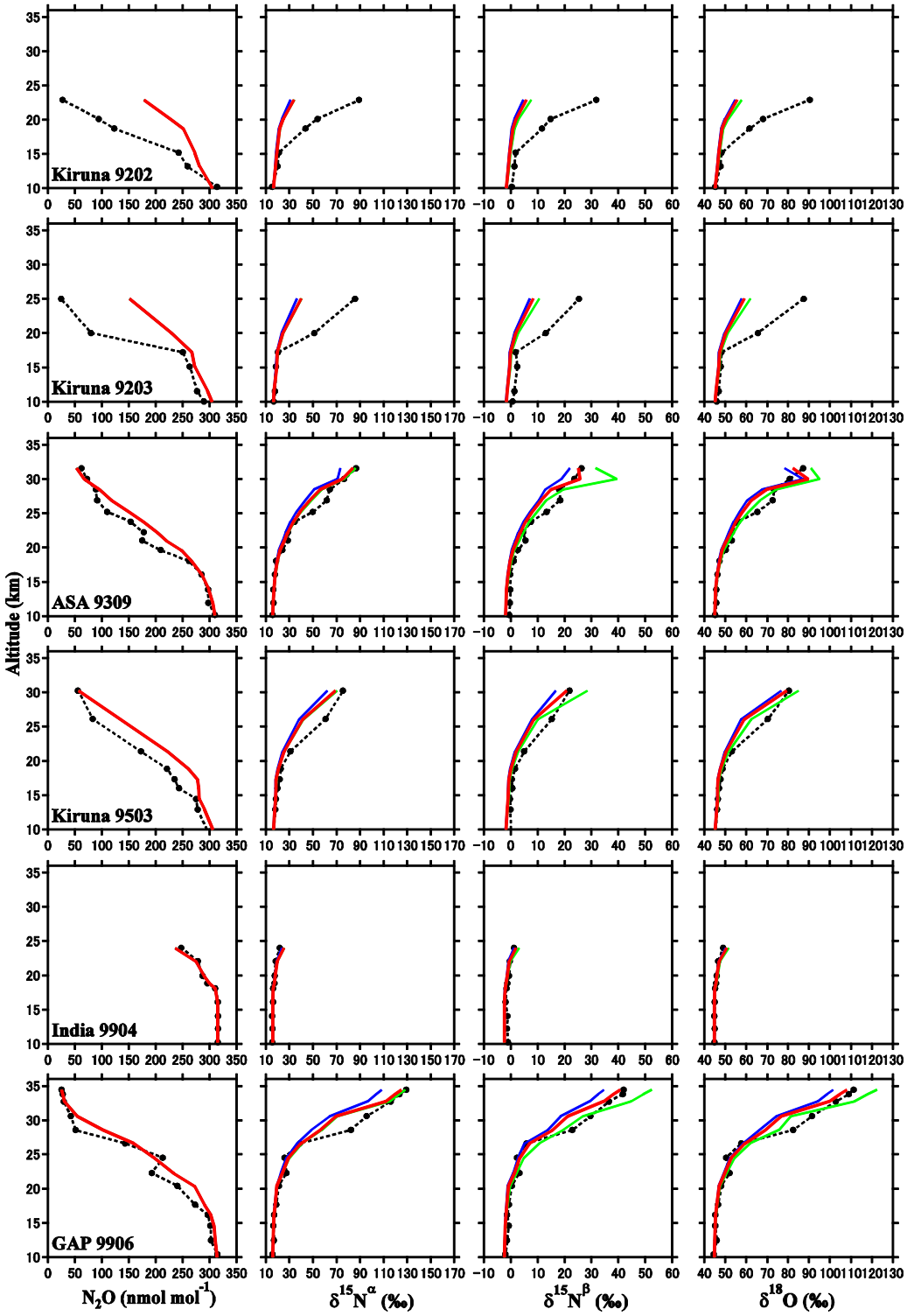
Kiruna 9202
Kiruna 9203
ASA 9309
Kiruna 9503
India 9904
GAP 9906
Altitude (km)
N2O (nmol mol-1)
δ15Nα (‰)
δ15Nβ (‰)
δ18O (‰)

Figure S2 (c).

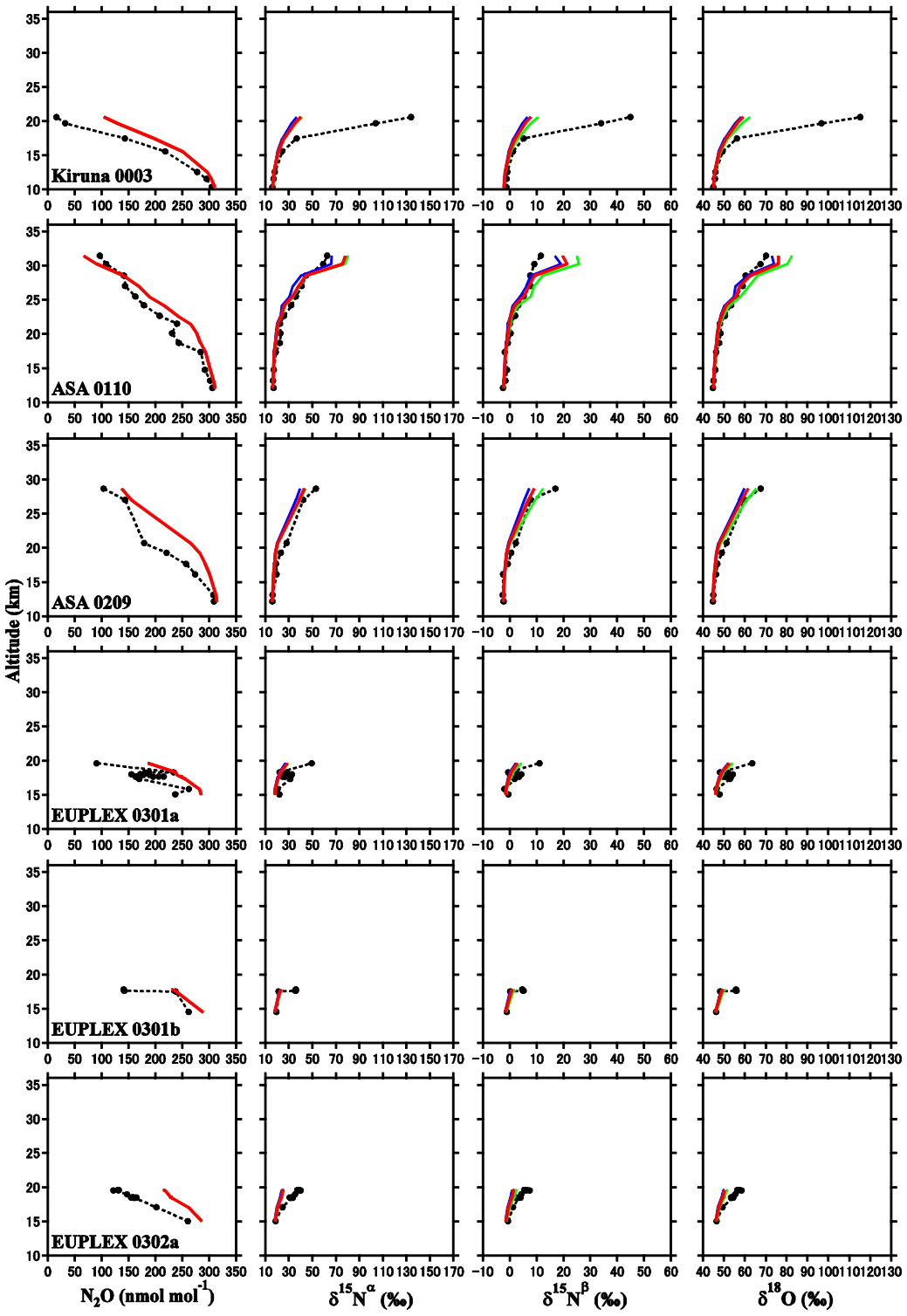

203

204

205 Figure S2 (d).

206

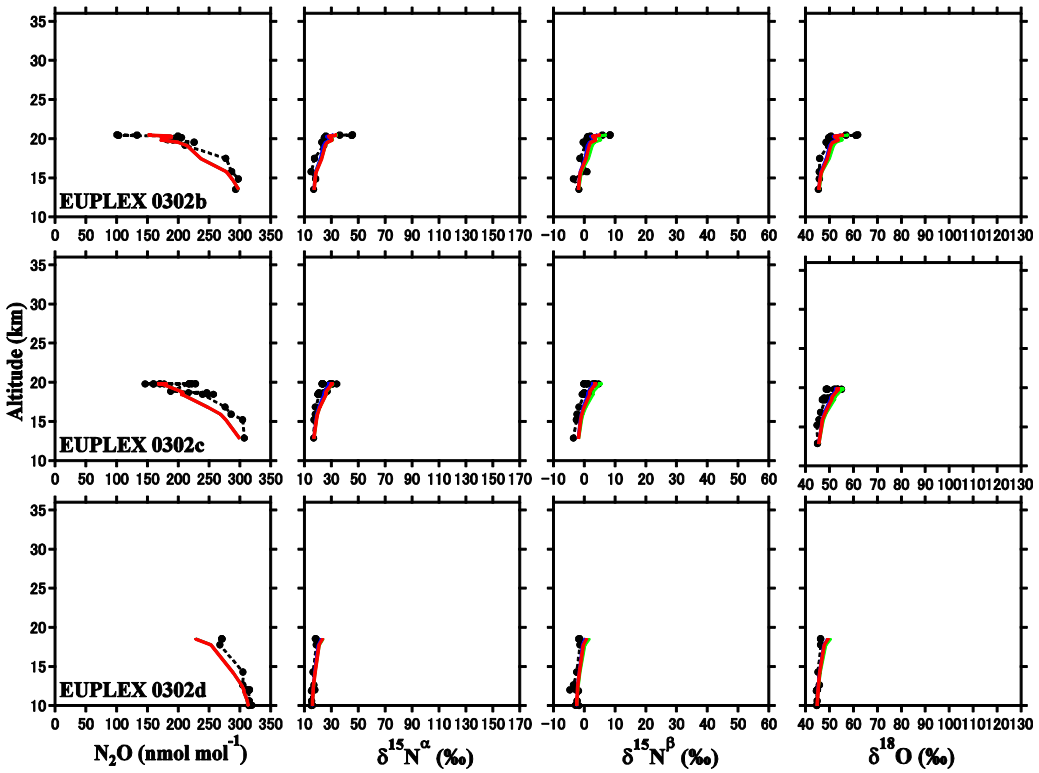

207

208

209 Figure S2 (e).

210

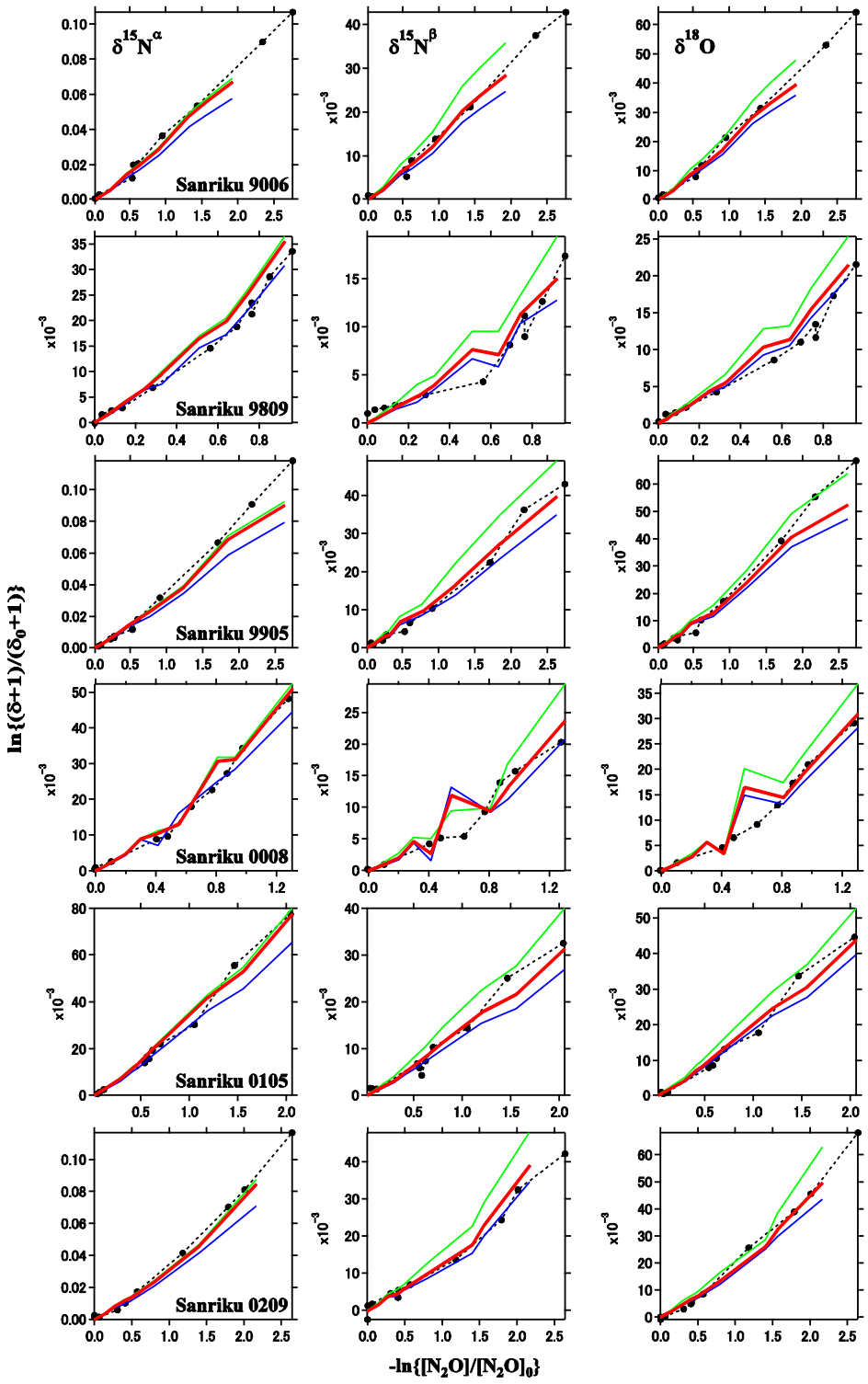

211

212

213 Figure S3 (a). Same as Fig. 4, but separately shown for each isotopic component from all
214 balloon and aircraft observations, which were used for the optimization of photolytic
215 fractionation in the model.

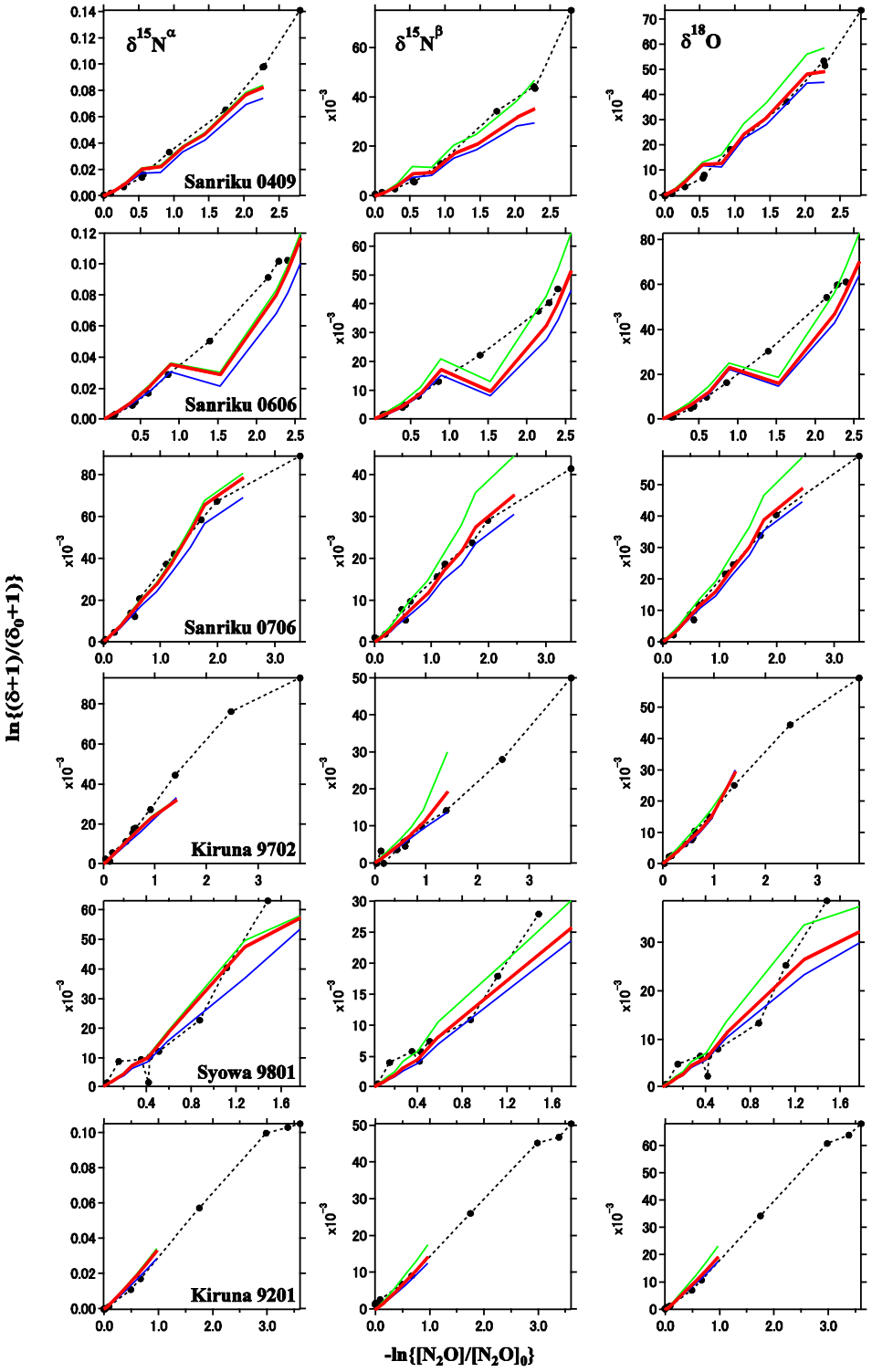
δ15Nα
δ15Nβ
δ18O
Sanriku 0409
Sanriku 0606
Sanriku 0706
Kiruna 9702
Syowa 9801
Kiruna 9201
x10-3
ln{(δ+1)/(δ0+1)}
-ln{[N2O]/[N2O]0}

Figure S3 (b).

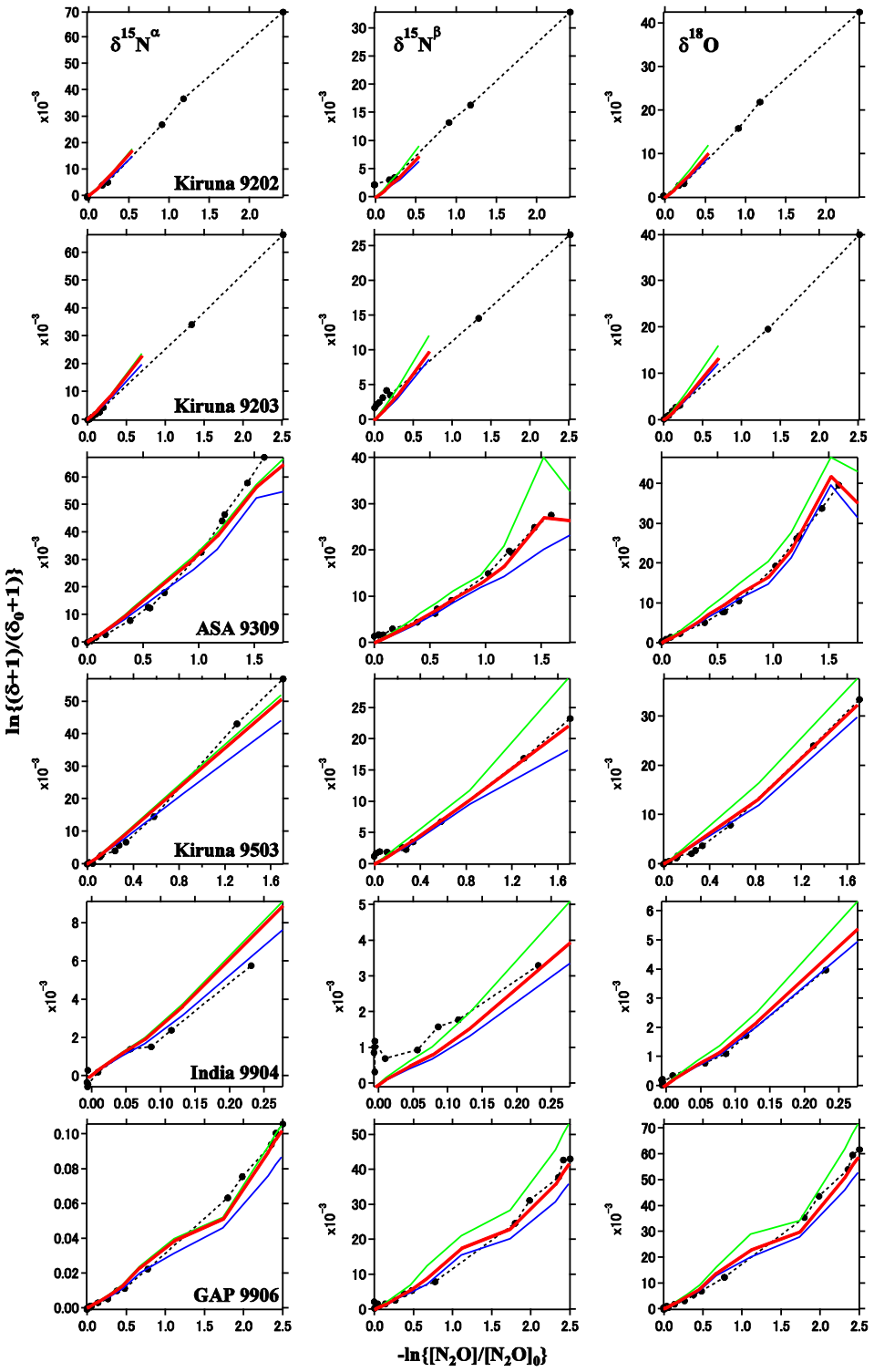

222

223

224 Figure S3 (c).

225

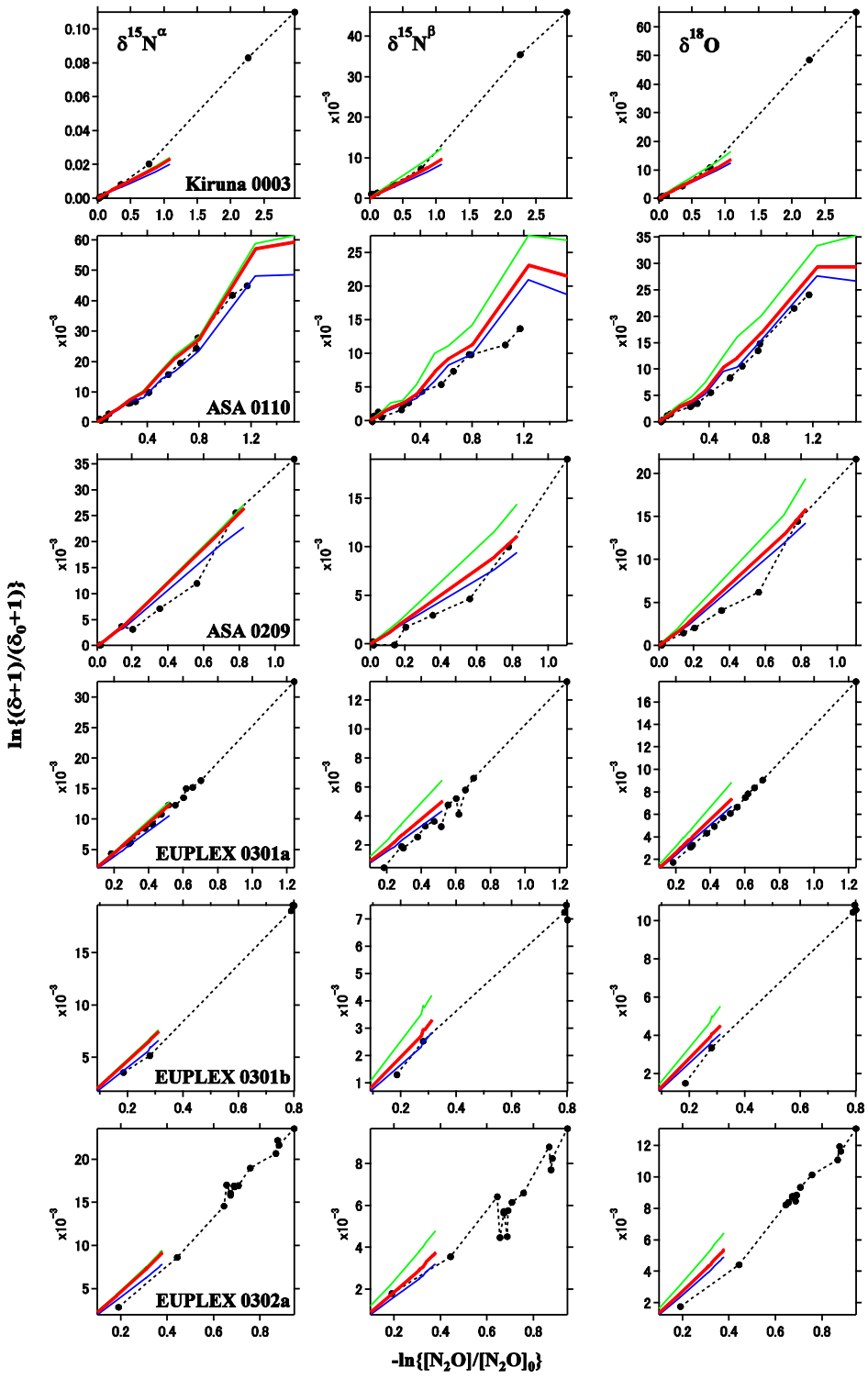

226

227

228 Figure S3 (d).

229

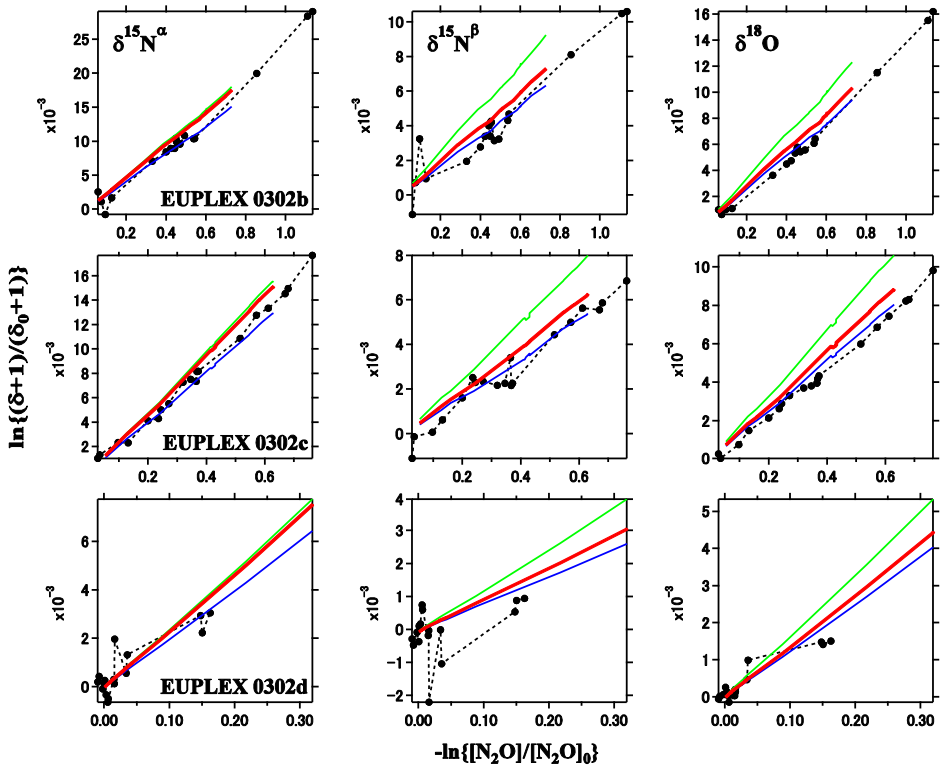

230

231

232 Figure S3 (e).

233

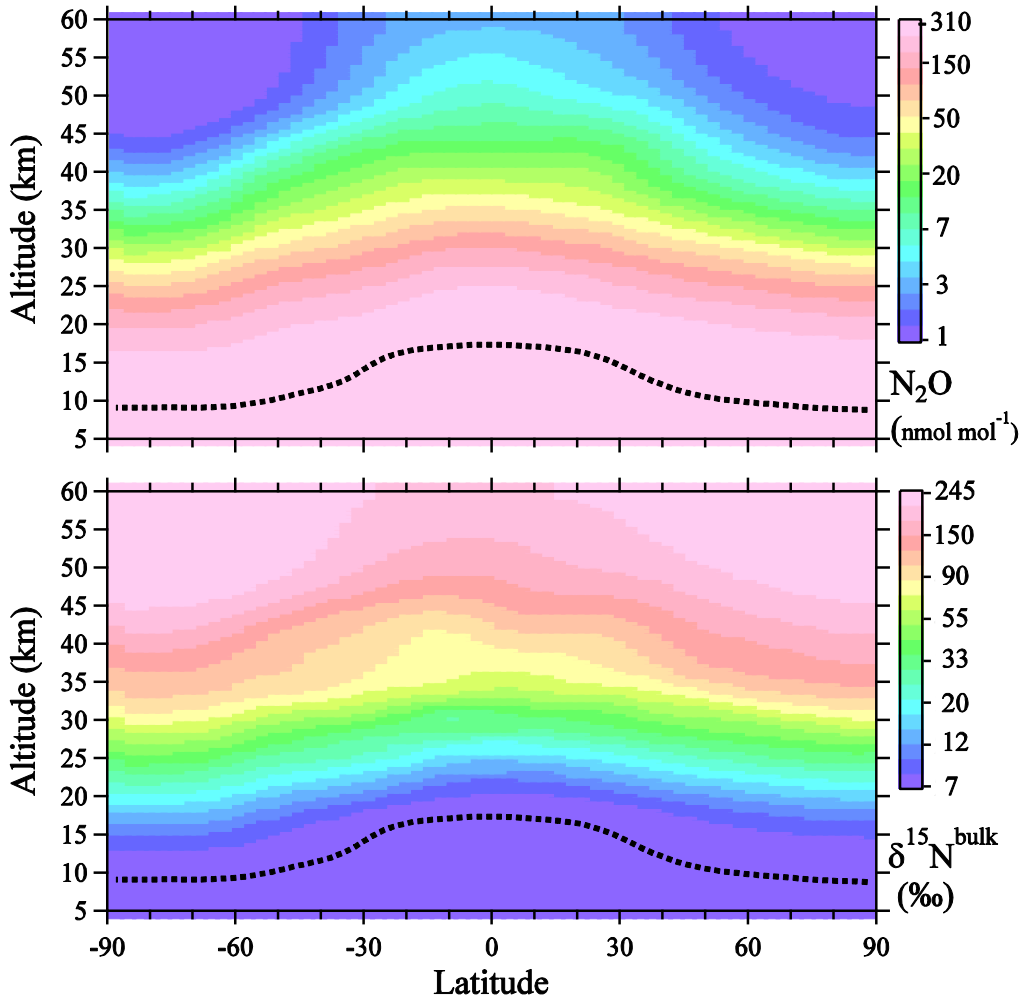

234

235

236 Figure S4. Same as Fig. 8, but in the altitude range of 5–60km.